JCBPS; Section C; August 2017 – October, 2017, Vol. 7, No. 4; 890-.899 E- ISSN: 2249 –1929
[DOI: 10.24214/jcbps.C.7.4.89099.]

Journal of Chemical, Biological and Physical Sciences

An International Peer Review E-3 Journal of Sciences

*Available online at*www.jcbsc.org

Section C: Physical Sciences

CODEN (USA): JCBPAT Research Article

Influence of Post Annealing on SnO_2 Nanoparticles and its Photocatalytic Activity in Methylene Blue Dye Degradation

P D Sahare[1] and Surender Kumar[2*]

[1]Department of Physics & Astrophysics, University of Delhi, Delhi

[2]Department of Physics, Ramjas College, University of Delhi, Delhi

Received: 15 August 2017**; Revised:** 31 August 2017; **Accepted:** 08 September 2017

Abstract: SnO_2 nanoparticles were synthesized using flux method. Synthesized SnO_2 nanoparticles were characterized for their structure and morphology using X-ray diffraction and scanning electron microscopy respectively. The average particle size of as synthesized SnO_2 nanoparticles was about 60 nm and the diameter of nanoparticles increases with increasing annealing temperature by keeping its spherical shape. Photocatalytic properties of as synthesized and annealed nanoparticles were studied for methyl blue organic dye under UV light. Pristine SnO_2 nanoparticles were found to be highly photocatalytic active and with increasing annealing temperature the photocatalytic activity decreases.

Keywords: Nanoparticles, degradation, photocatalysis, surface defects.

INTRODUCTION

Now days, wastewater has become a prime concern of the environment due to its increasing quantity and variety. There are many factors responsible for discharging wastewater in vast amount, but textile industries are dominant among them. These industries release organic dye wastes without proper treatment and handling, which generates environmentally hazardous pollutants. In particular, 15% of organic dye of total production of world is lost during the dyeing process and is ejected in the form of industrial waste, which ultimately pollutes the surface and ground water. The hazardous pollutants discharging from industries contain organic dyes which require special refinement processes because of their non-self-degradable nature. These wastes in the ecosystem are a major source of eutrophication,

nonaesthetic pollution and perturbations in the marine life. Therefore, the treatment of wastewater is an essential measure in environmental safety[1].

For the treatment of wastewater a range of biological, physical and chemical methods are used[2,3]. Biological treatment of wastewater is an established technology and is inexpensive. However, it is well known that the majority of organic dyes are not degraded by biological method because it gets adsorbed on the sludge. Physical methods consist of adsorption, ion-exchange, air stripping, etc. but the major difficulty with these methods is that they transfer the contamination from one phase to another i.e., not destructive method. Therefore a new kind of treatment is required which should be destructive in nature and can act on these pollutants significantly.

Chemical photocatalysis at the surface of metal oxide semiconductor utilize visible or UV light to produce and use hydroxyl free radicals (OH^-) as strong oxidant that can react with organic dye pollutants and destroy it[4,5]. Such chemical treatment is simpler and much more efficient than the physical and biological methods. This photocatalysis technique has attracted distinct interest from science community as the most promising method to getting rid of residual dyes pollutants from wastewater stream[6]. For photocatalysis at least two reactions must happening simultaneously, the first reaction is oxidation, from photo-induced positive holes, and the second one involving reduction, from photo-induced negative electrons[7]. Several types of promising photocatalyst, such as zinc oxide (ZnO), zirconia (ZrO_2), iron(III) oxide (Fe_2O_3), niobium pentoxide (Nb_2O_5), vanadium(V) oxide (V_2O_5), and tungsten trioxide (WO_3), titanium dioxide (TiO_2), and SnO_2 have been actively applied in environmental waste management system[8,9].

Among them SnO_2 is considered to be one of the best metal oxide semiconductor, has been used in many aspects such as transparent conducting oxide, sensors, photocatalysis, because of its optically transparency for visible range of electromagnetic spectrum, high chemical stability, easy availability, nontoxicity and high redox potential of generation of electron hole (e-h) pairs[5,10,11]. The nanostructures of SnO_2 with different morphology, such as nanotubes, nanorods, nanospheres, and nanoparticles, have been studied, and great advancements has been made in recent years[12,13]. The nanoparticles have large surface area to volume ratio, which is directly correlated to many physicochemical properties such as chemical reactivity, surface adsorption ability, and surface charge and therefore gain significant attention in the field of photocatalysis. It is important to realise that photogenerated e-h pair recombination can occur via surface states (surface recombination), and clearly this pathway will be particularly important for systems such as nanoparticles with very high surface area to volume ratios. Doped SnO_2 with cation or anion are becoming popular, because doping has its own advantages for different applications, however, doping create defects levels within the band gap of semiconductor material and causes trapping sites for photogenerated e-h pairs and decreases its photocatalytic activity[14].

In this work, nanoparticles of SnO_2 were synthesized using flux method and the photocatalytic activity is investigated by evaluating the photocatalytic degradation of the methylene blue (MB) dye aqueous solution at room temperature. Photocatalysis results demonstrate that the pristine SnO_2 nanoparticles decolorizes MB organic dye faster than the annealed samples under UV light irradiation and the solution turn colourless within 40 minutes of irradiation time. We present the Raman and FTIR spectra of SnO_2 nanoparticles to understand various native defects and their role in photo degradation of organic dye. We also present the observations of annealing temperature effects on structural, morphological, optical, and photocatalytic properties.

EXPERIMENTAL

SnO_2 nanoparticle synthesis using Flux method: SnO_2 nanoparticles were synthesized by flux method using tin chloride dihydrate ($SnCl_2 \cdot 2H_2O$) and sodium hydroxide (NaOH) as precursor material. The

$SnCl_2 \cdot 2H_2O$ (2.26 g, 10 mmol) and NaOH (0.8 g, 20 mmol) were ground with a mortar and pestle for 20 min. Then, sodium chloride (NaCl) was added to the mixture at a molar ratio of 1:2 and further ground for another 30 min. The mixture was then oxidized by annealing in air for 2 h at 400 ºC. The final products were washed with water and ethanol several times and dried for 12 h at 60 ºC. This synthesis method produced a high yield of SnO_2 nanoparticles. The obtained nanoparticles are divided into 5 parts. One part is kept as a pristine sample while other parts are annealed at different temperature as 600, 800, 1000, 1200 ºC for five hours in air then used for further characterisations.

Characterizations: X-ray diffraction (XRD) patterns of SnO_2 nanoparticles were carried out using Cu Kα radiation (λ= 1.54056 Å) on "Bruker D8" X-ray diffractometer, for 2θ ranging from 20° to 70°. For surface morphology study scanning electron microscope (SEM) images were taken on QUANTA, 200F, FEI. Raman spectroscopic was carried out using Renishaw In Via Reflex micro Raman spectrometer consisting of air cooled argon laser having wavelength ~514.5 nm as a source. Fourier Transformation Infrared (FTIR) spectra were recorded by Perkin-Elmer spectrometer.

Photocatalytic Experiment*:* Photocatalytic studies were carried out in an immersion-type, in-house fabricated photochemical reactor consenting of UV-lamp (λ≤380 nm), magnetic stirrer, double walled quartz jacket and Pyrex glass reactor as shown in Fig. 1. A high-pressure mercury vapor lamp of 125W (Philips made, India) is placed inside the double-lined quartz tube jacket having dimensions of 3.5 cm inner diameter, 4.5 cm outer diameter and 20 cm height . Then this quartz jackets is placed inside Pyrex glass reactor having dimension 14 cm inner diameter, 16 cm outer diameter and 20 cm height. The Pyrex glass reactor and double walled quartz jacket was maintain at room temperature by circulating water continuously during the photochemical reaction in addition to this it also act as an IR filter. An aqueous solution of MB dye along with desired amount of SnO_2 nanoparticles (catalyst) is taken in Pyrex container and was constantly stirred to maintain a homogeneous suspension.

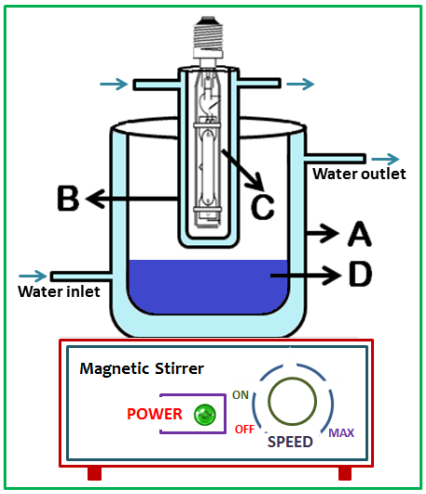

Figure 1: Schematic diagram of photochemical reactor consisting of (A) Double walled Pyrex container (B) double walled quartz jacket (C) high pressure mercury vapor lamp (d) MB organic dye solution.

RESULTS AND DISCUSSIONS

Structural and morphological investigations: Figure 2 show the XRD patterns of SnO_2 nanoparticles pristine and annealed at different temperatures. Results shows that all the samples have tetragonal rutile structure and are well matched with the standard JCPDS: 41-1445. The crystallinity of the SnO_2 particles

increase with annealing temperatures as observed from the decrease in the full width at half maximum (FWHM) value and increase in the intensity of the XRD patterns. Furthermore, no peaks corresponding to any other phase or contamination is found in the recorded diffractograms. The average crystallite size is estimated using FWHM value from the line broadening of the XRD peaks using Scherrer's formula:

$$D = 0.9\lambda/\beta \cos\theta \qquad (1)$$

Where, D is the average crystallite size, λ is the incident wavelength, θ is the Bragg angle, and β is the diffracted FWHM (radian). The average crystallite sizes of the samples are 63, 150, 176, 193 and 244 nm for the pristine, samples annealed at 600, 800, 1000 and 1200 °C, respectively, as expected, from the sharpened and enhanced diffraction peaks. The FWHM and average crystallite size has been calculated from the XRD plot for each pattern and presented in Figure 3 as a function of annealing temperature.

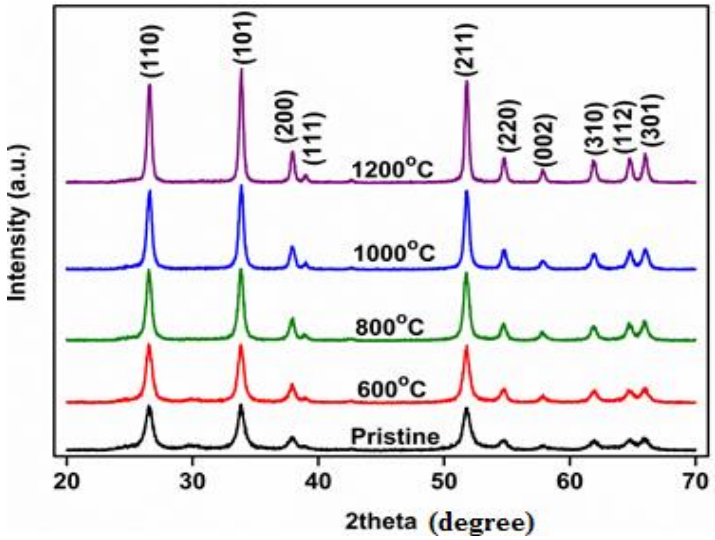

Fig. 2: XRD patterns of SnO_2 nanoparticles annealed at different temperatures.

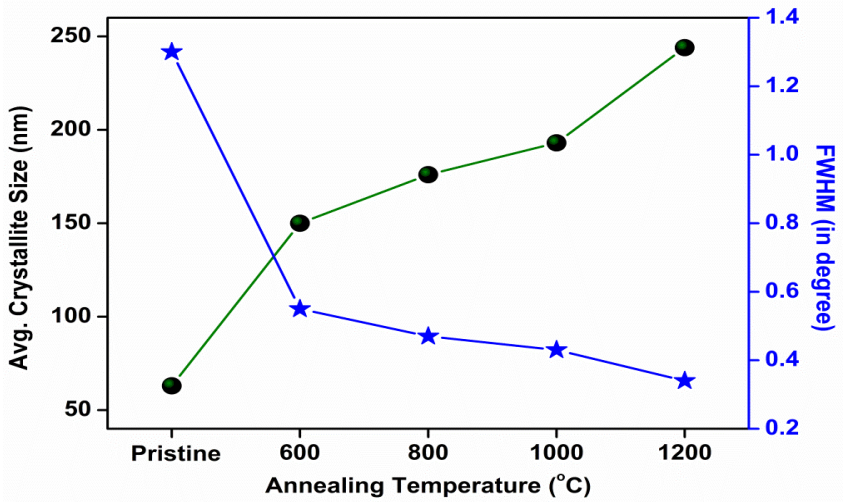

Fig. 3: Show the average crystallite size and FWHM (from XRD (101) peak) of SnO_2 samples as a function of annealing temperature.

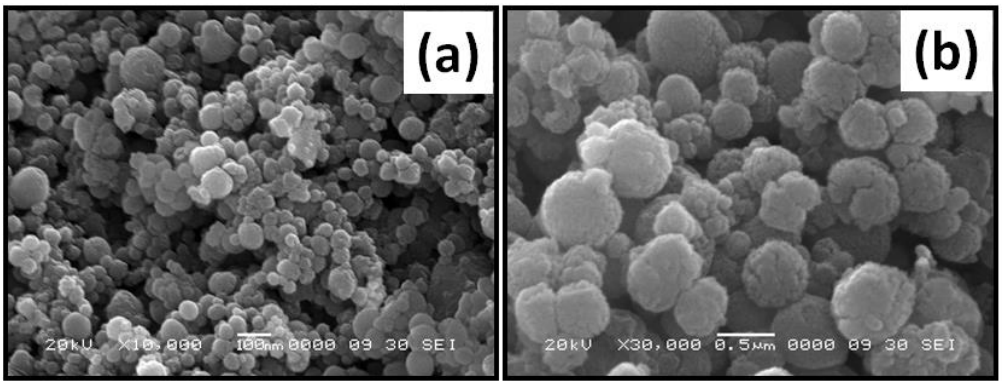

Fig. 4: SEM images of SnO_2 samples (a) pristine and (b) annealed at 1200 ºC.

Figure 4 shows the SEM images of the SnO_2 nanoparticles. Fig. 4 (a) shows the SEM image of pristine SnO_2 nanoparticles composed of almost spherical shaped nanoparticles with diameter around 80 nm. Fig. 4 (b) shows the SEM image of annealed (at 1200 ºC) sample having particle diameter around 0.5 µm. From Figure 4 (a) and 4 (b) it can be inferred that with annealing temperature, the particle size increases but the shape of the particles remain spherical. It is found that the particle size increased from around 80 nm to around 0.5 µm with an annealing temperature (1200 ºC), indicating that the surface to volume ratio of SnO_2 particles decreased[15]

Optical studies

Raman Spectroscopy: Figure 5 show graph for Raman spectroscopy measurements. It is well-known that SnO_2 has a tetragonal rutile crystalline structure and that its unit cell consists of two tin atoms and four oxygen atoms with a space group $D_{4h}^{14}(P4_2/mnm)$. Six unit cell atoms give a total of 18 vibrational modes in the first Brillouin Zone. The mechanical representation of the normal modes at the center of the Brillouin zone is given by[16]

$$\Gamma=\Gamma_1^+(A_{1g}) + \Gamma_2^+(A_{2g}) + \Gamma_3^+(B_{1g}) + \Gamma_4^+(B_{2g}) + \Gamma_5^-(E_g) + 2\Gamma_1^-(A_{2u}) + 2\Gamma_4^-(B_{1u}) + 4\Gamma_5^+(E_u) \qquad (2)$$

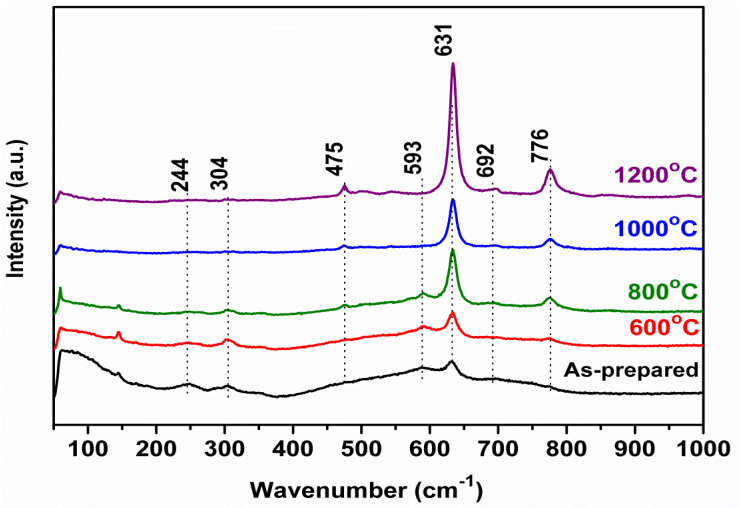

Fig. 5: Raman spectra of SnO_2 samples, annealed at different temperatures.

Here the Koster notations with commonly used symmetry designations are listed in parentheses. The modes A_{1g}, B_{1g}, B_{2g} and E_g are Raman active while A_{2u} and E_u are infrared active. Similarly, A_{2u} and E_u

modes are TO and LO, respectively. The room temperature Raman spectra of all the samples of the present investigation are shown in Fig. 5.

These Raman spectra are found to be similar to that of as-prepared SnO_2. It is interesting to note that by annealing the SnO_2 lattice, the intensities of higher wavenumber Raman peaks are found to increase, indicating that annealing might be responsible for the changes in local disorder and defects such as vacant lattice sites or vacancy cluster or local disorder. This may result in lattice distortion and reduction in lattice space symmetry. Further, the most intense peak observed at 631 cm^{-1} in the case of pristine SnO_2 may be attributed to the A_{1g} mode, while those exhibited at 475 and 776 cm^{-1} may be attributed to vibrational modes E_g and B_{2g}, respectively. The modes A_{1g} (~631 cm^{-1}) and B_{2g} (~776 cm^{-1}) might be related to the expansion and contraction of the vibrating mode of Sn-O bonds, while the E_g mode may be related to the vibration of oxygen in the oxygen plane. Apart from this, both the as-prepared and annealed samples are found to exhibit two more bonds with less intensity between 304 and 692 cm^{-1} and may not be assigned to parasitic phases in the SnO_2 lattice[17, 18]. In addition to these peaks, some extra ones have been observed at 244 and 593 cm^{-1} and the observation of these new peaks may be explained as follows. In the nanocrystalline SnO_2 based system, as the surface properties are sensitive not only to the grain size and their distributions but also to the oxygen vacancies and local disorder, there may be a possibility of the appearance of new modes in the Raman spectra[19, 20]. The Raman peaks' data are found to be comparable with those available in the literature[21, 22]. Further, a continuous detraction of the FWHM of Raman peaks with increasing crystallite size observed in the samples of the present investigation may be due to phonon confinement effect, and such a phenomenon was reported earlier in many nanocrystalline materials such as TiO_2, ZnO, CeO_2, etc.[23, 24.]

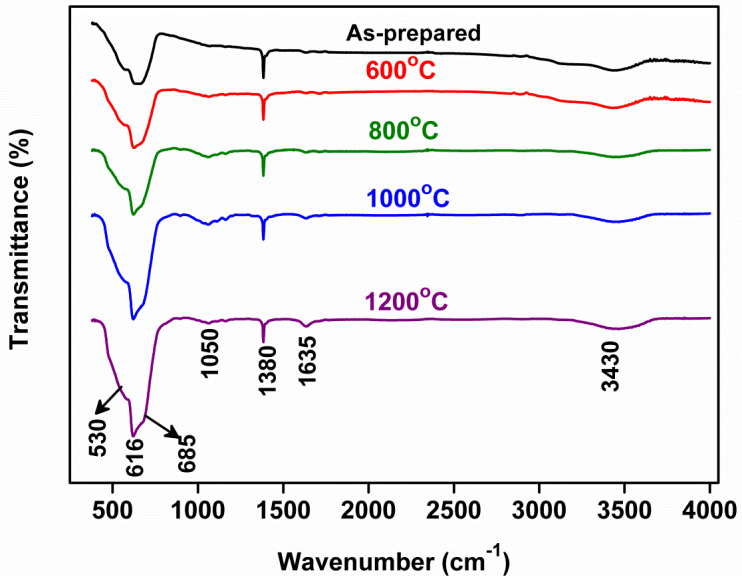

Fig.6: FTIR spectra of SnO_2, annealed at different temperatures

Figure 6 shows the room temperature FTIR spectra of SnO_2 nanoparticles in the range of 380-4000 cm^{-1} in transmission mode. The bands exhibited in the low wavenumber region of 474-620 cm^{-1} might be due to vibration of antisymmetric Sn-O-Sn mode of tin oxide, while a lattice mode due to SnO_2 appears in the region 685-725 cm^{-1}. It is also interesting to note that the width of Sn-O-Sn band decreases while that of O-Sn-O band increases with increasing annealing temperature, and the observed behaviour may be attributed to the improvement in crystallinity due to the removal of residual organic impurities and

increase of oxygen content. The bands appearing in all the samples around 1635 cm^{-1} may be attributed to the bending mode of O-H bonds. The broad band appearing in the region 3000-3700 cm^{-1} is found to decrease gradually with increasing annealing temperature and may be due to vibration of adsorbed water. These observations are in agreement with those reported earlier[25]. The strong IR band 1050 cm^{-1} were assigned as the vibrational mode of (O-H) group and the other band at 1380 cm^{-1} were attributed to metal hydroxide networking (Si-OH or Sn- OH) in the samples.

Photocatalytic studies: Figure 7 (a) shows the absorption spectra of MB dye (the maximum absorbance at around 665 nm) with pristine SnO_2 nanoparticle under UV light irradiation for different time interval (0 to 40 minutes). It reveals from the UV absorption spectra that with increasing photocatalytic reaction time the absorption of MB dye diminish and in 40 minutes it becomes zero. It infers that within 40 minutes of photocatalysis reaction the MB dye gets completely degraded. In Figure 7 (b) it is clearly seen that in the presence of SnO_2 nanoparticles, the absorbance decreased initially, indicating adsorption of the dye MB (in the dark). It may be noted here that the decrease in the absorption intensity (in dark) is not due to the degradation but due to removal of the adsorbed MB dye on the surface of the catalyst (in the dark without any irradiation) before the UV-visible measurements. Further, a substantial decrease in the absorbance of MB was observed after conducting the reaction under UV irradiation with increasing time. The solution turned out colourless within 40 min of irradiation while using pristine SnO_2 nanoparticles as catalyst. A similar experiment was carried out for annealed (800 and 1200 ^oC) SnO_2 samples as well for a comparative study.

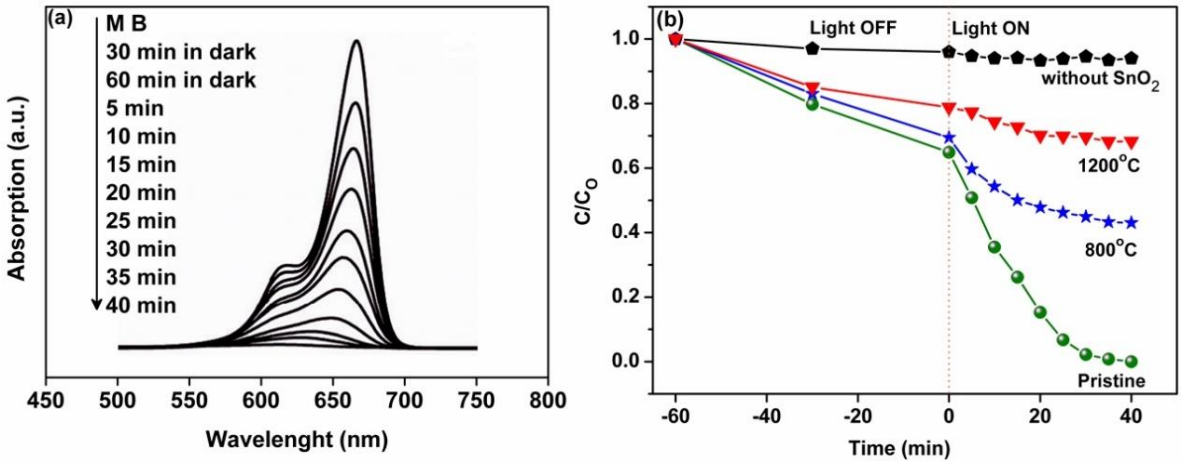

Figure 7:(a) Show the absorption spectra of MB dye solution for different duration of photochemical reaction, (b) photocatalysis of MB dye under UV irradiation with and without SnO_2 nanoparticles.

These results clearly demonstrated that pristine SnO_2 sample decolorizes MB dye faster than annealed samples under similar experimental conditions. This is attributed to the smaller particle size and new defect sites (or recombination centers) that enhance the recombination of photogenerated electrons and holes of SnO_2 samples. Yu et al. also show annealed samples has a lesser photocatalytic activity due to the small surface area as compared to pristine samples which introduction of new defect sites that enhances the recombination of photogenerated electrons and holes[26]. Secondly, the smaller particle size of pristine sample shows an enhanced photocatalytic activity due its large surface area to volume ratio and high surface reactivity. In particulate systems, a decrease in the average particle size is expected to increase the rate of interfacial charge transfer. A lower particle size increases the specific surface area and thus increases the number of active surface sites where the photogenerated charge carriers are able to react with absorbed molecules to form hydroxyl and superoxide radicals. For a sufficiently small particle

size, surface recombination becomes the dominant process as the charge carriers are formed close to the particle surface and also because the recombination process is faster than interfacial charge transfer[27,28].

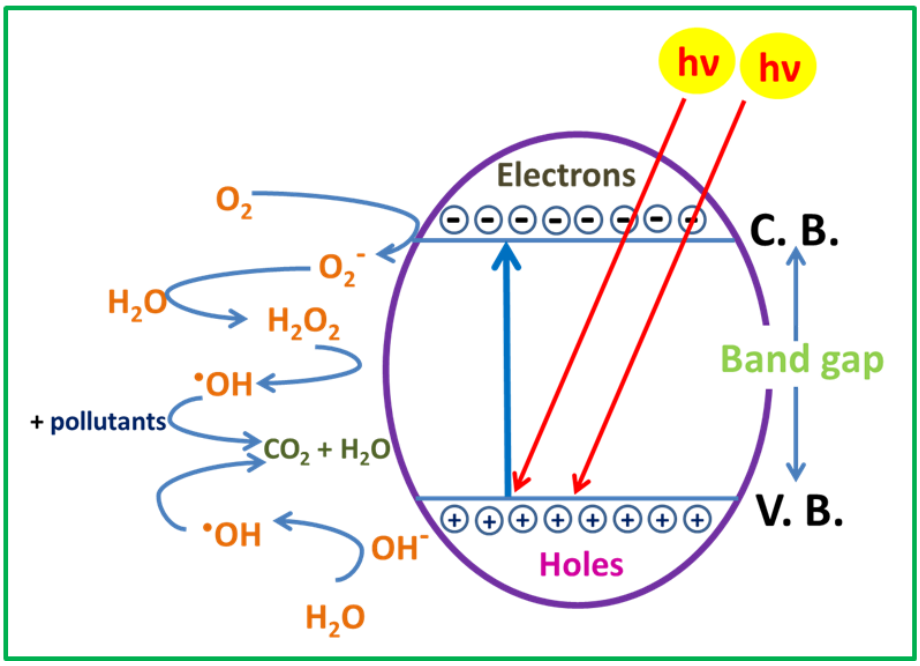

Figure 8: Schematic diagram of the principle of photocatalysis

Figure 8 shows a schematic diagram of the mechanism involved in photocatalysis reaction with SnO_2 nanoparticles. UV light is an ionizing radiation and it acts on the catalyst, the dye, and the solvent simultaneously. It creates electron-hole pairs in the SnO_2 nanoparticles, sensitizes the MB organic dye by exciting it to singlet/triplet states and generates free electrons by breaking some of the bonds and helps in generating H_2O_2 and OH^- radicals in the solvent for further catalysis and degradation of the MB dye.

$$H_2O + h^+ \rightarrow H^+ + OH^\bullet \quad (3)$$

$$MB + h\nu \rightarrow MB^* \quad (4)$$

$$MB^* + h\nu \rightarrow MB^{+\bullet} + SnO_2\,(e^-) \quad (5)$$

$$SnO_2\,(e^-) + O_2 \rightarrow SnO_2 + O^{2-} \quad (6)$$

$$SnO2\,(e^-) + O^{2-} + H^+ \rightarrow H_2O_2 \quad (7)$$

$$H_2O_2 + h\nu \rightarrow OH^\bullet \quad (8)$$

$$MB + OH^\bullet \rightarrow CO_2 + H_2 \quad (9)$$

The electrons the holes generated due to ionization of SnO_2 nanoparticles can participate in some reactions as shown in Equations 3 to 9 assisted by the O_2 (dissolved in water) and H_2O_2 (formed due to catalysis) respectively, to generate many OH^- (hydroxyl radicals), which has strong oxidizing ability and are available to oxidize many organic intermediates to form CO_2 as the final product which gets finally liberated in the atmosphere.

CONCLUSION

The synthesis of SnO_2 nanoparticles is successfully carried out by flux method. The XRD and Raman results indicates that the synthesized sample have rutile crystal structure with space group $D_{4h}^{14}(P4_2/mnm)$. The average diameter of the nanoparticles is estimated by using Scherrer's formula and SEM images and it is found that they are in good agreement with each other. It is found that the pristine SnO_2 nanoparticles have very high photocatalytic activity; it decolonizes the MB dye within 40 minutes of photolytic reaction under UV light irradiation. Furthermore, samples annealed at 800 and 1200 ºC samples decolourise MB dye 60 and 30 % respectively which is very much slower than corresponding pristine sample.

ACKNOWLEDGMENTS

We are thankful to the University of Delhi for providing research facilities at USIC.

REFERENCES

1. P.C. Vandevivere, R. Bianchi, W. Verstraete, Treatment and reuse of wastewater from the textile wet-processing industry: Review of emerging technologies, J. Chem. Technol. Biotechnol,1998, 72, 289–302.
2. E.J. Bouwer, P.B. Crowe, Biological Processes in Drinking Water Treatment, J. Am. Water Works Assoc,1988, 80, 82–93.
3. V.K. Gupta, I. Ali, T.A. Saleh, A. Nayak, S. Agarwal, Chemical treatment technologies for waste-water recycling—an overview, RSC Adv. 2 ,2012, 6380-6388.
4. E. Borgarello, J. Kiwi, E. Pelizzetti, M. Visca, M. Grätzel, Photochemical cleavage of water by photocatalysis, Nature,1981, 289,158–160.
5. A. Ibhadon, P. Fitzpatrick, Heterogeneous Photocatalysis: Recent Advances and Applications, Catalysts, 2013, 3,189–218.
6. D.R. Jones, V. Gomez, J.C. Bear, B. Rome, F. Mazzali, J.D. McGettrick, A.R. Lewis, S. Margadonna, W.A. Al-Masry, C.W. Dunnill, Active removal of waste dye pollutants using $Ta_3N_5/W_{18}O_{49}$ nanocomposite fibres, Sci. Rep.,2017, 7,4090 (1-16).
7. A. Fujishima, K. Honda, Electrochemical Photolysis of Water at a Semiconductor Electrode, Nature, 1972, 238, 37–38.
8. M.M. Mahlambi, C.J. Ngila, B.B. Mamba, Recent Developments in Environmental Photocatalytic Degradation of Organic Pollutants : The Case of Titanium Dioxide Nanoparticles A Review, J. Nanomaterials. 2015 1–29.
9. M.A. Johar, R.A. Afzal, A.A. Alazba, U. Manzoor, Photocatalysis and Bandgap Engineering Using ZnO Nanocomposites, 2015, 1-22.
10. X. Pan, Z. Yi, Graphene Oxide Regulated Tin Oxide Nanostructures: Engineering Composition, Morphology, Band Structure, and Photocatalytic Properties, ACS Appl. Mater. Interfaces, 2015, 7, 27167–27175.
11. S.H. Lee, D.M. Ho, A.J. Jacobson, T.R. Lee, Transparent, Homogeneous Tin Oxide (SnO_2) Thin Films Containing SnO_2 Coated Gold Nanoparticles, Chem. Mater.2013, 25, 4697–4702.
12. H. Wang, A.L. Rogach, Hierarchical SnO_2 Nanostructures: Recent Advances in Design, Synthesis, and Applications, Chem. Mater.2014, 26, 123-133.
13. N. Talebian, F. Jafarinezhad, Morphology-controlled synthesis of SnO_2 nanostructures using

hydrothermal method and their photocatalytic applications, Ceram. Int.2013, 39, 8311–8317.

14. Y.N. Tan, C.L. Wong, A.R. Mohamed, An Overview on the Photocatalytic Activity of Nano-Doped-TiO_2 in the Degradation of Organic Pollutants, ISRN Mater. Sci. 2011, 1–18.
15. W. Ke, D. Zhao, A.J. Cimaroli, C.R. Grice, P. Qin, Q. Liu, L. Xiong, Y. Yan, G. Fang, Effects of annealing temperature of tin oxide electron selective layers on the performance of perovskite solar cells, J. Mater. Chem. A.2015, 3, 24163–24168.
16. J.G. Traylor, H.G. Smith, R.M. Nicklow, M.K. Wilkinson, Lattice dynamics of rutile, Phys. Rev. B. 3,1971, 3457–3472.
17. A. Bouaine, N. Brihi, Structural , Optical , and Magnetic Properties of Co-doped SnO_2 Powders Synthesized by the Coprecipitation Technique, J. Phys. Chem. C.2007, 111, 2924–2928.
18. J.X. Zhou, M.S. Zhang, J.M. Hong, Z. Yin, Raman spectroscopic and photoluminescence study of single-crystalline SnO_2 nanowires, Solid State Commun.2006, 138, 242–246.
19. D.L. Hou, H.J. Meng, L.Y. Jia, X.J. Ye, H.J. Zhou, X.L. Li, Oxygen vacancy enhanced the room temperature ferromagnetism in Ni-doped TiO_2 thin films, Phys. Lett. Sect. A Gen. At. Solid State Phys., 2007,364, 318–322.
20. Z.W. Chen, J.K.L. Lai, C.H. Shek, Insights into microstructural evolution from nanocrystalline thin films prepared by pulsed laser deposition, Phys. Rev. B.,2004, 70,165314.
21. S.H. Sun, G.W. Meng, G.X. Zhang, T. Gao, B.Y. Geng, L.D. Zhang, J. Zuo, Raman scattering study of rutile SnO_2 nanobelts synthesized by thermal evaporation of Sn powders, Chem. Phys. Lett.2003, 376,103–107.
22. C. Xie, L. Zhang, C. Mo, Characterization of Raman spectra in nano-SnO_2 solids, Phys. Status Solidi.1994, 141, K59–K61.
23. I.H. Campbell, P.M. Fauchet, The effects of microcrystal size and shape on the one phonon Raman spectra of crystalline semiconductors, Solid State Commun. 1986, 58, 739–741.
24. J.E. Spanier, R.D. Robinson, F. Zhang, S.-W. Chan, I.P. Herman, Size-dependent properties of nanoparticles as studied by Raman scattering, Phys. Rev. B. 2001, 64, 245407.
25. J.X. Zhou, M.S. Zhang, J.M. Hong, J.L. Fang, Z. Yin, Structural and spectral properties of SnO_2 nanocrystal prepared by microemulsion technique, Appl. Phys. A Mater. Sci. Process.2005, 81,177–182.
26. J.C. Yu, J. Yu, W. Ho, Z. Jiang, L. Zhang, Effects of F-doping on the photocatalytic activity and microstructures of nanocrystalline TiO_2 powders, Chem. Mater. 2002, 14, 3808–3816.
27. A.C. Dodd, A.J. McKinley, M. Saunders, T. Tsuzuki, Effect of particle size on the photocatalytic activity of nanoparticulate zinc oxide, J. Nanoparticle Res.2006, 8, 43–51.
28. N. Padmavathy, R. Vijayaraghavan, Enhanced bioactivity of ZnO nanoparticles—an antimicrobial study, Sci. Technol. Adv. Mater.2008, 9,35004 (1-7).

*** Corresponding author: Surender Kumar;**

2Department of Physics, Ramjas College, University of Delhi, Delhi

Online publication Date: 8.9.2017